

## A Moore-Greitzer Model for Ducted Fans in Ground Effect

Y. Jin, Y. Fu, Y. Qian and Y. Zhang<sup>†</sup>

*State Key Laboratory of Automotive Safety and Energy, Tsinghua University, Beijing, 100084, China*

*<sup>†</sup>Corresponding Author Email: yjzhang@tsinghua.edu.cn*

(Received June 18, 2019; accepted August 3, 2019)

### ABSTRACT

Ducted fans are widely used in unmanned aerial vehicles due to their high propulsive efficiency and safety. The aerodynamics are complex within the vicinity of the ground, including take-off, landing and hovering. In the present study, the aerodynamic stability of the ducted fan was studied with a modified Moore-Greitzer model to estimate and analyse the stability in ground effect. The model was validated and compared with three-dimensional unsteady simulations. The results indicated that the rotating stall occurred for the ducted fan in ground effect. The model results can be used to guide the design and control of the vehicles, to ensure the stability and safety of both the ducted fan and vehicles.

**Keywords:** Ducted fan; Ground effect; Stability model; Unsteady simulation.

### NOMENCLATURE

$A_c$	fan duct area	$U_d$	input target of blade speed at mean radius
$a$	reciprocal time-lag parameter of blade passage	$V_p$	volume of plenum
$a_s$	sound speed	$W$	semi-width of cubic characteristic
$B$	$= U_d / (2a_s) \cdot \sqrt{V_p / (A_c L_c)}$	$\Gamma$	dimensionless torque of fan blade
$b$	$2a_s \sqrt{(A_c L_c) / V_p}$	$\gamma_T$	throttle coefficient
$H$	semi-height of cubic axisymmetric characteristic	$\theta$	angular coordinate around fan
$H_{GE}$	distance between duct outlet and ground	$\Lambda_1$	constant
$h$	dimensionless height	$\Lambda_2$	constant
$I$	fan blade moment of inertia	$\xi$	dimensionless time
$J$	square of amplitude of angular disturbance of axial-flow coefficient	$\rho$	density
$l_c$	total aerodynamic length of fan and duct, in blade tip radius	$\sigma$	slip factor of fan, tangential velocity of fluid at blade tip outlet divided by blade velocity
$l_E, l_I$	length of exit and entrance, in blade tip radius	$\tau$	coefficient of pressure-rise lag
$m$	fan-duct flow parameter	$\tau_t$	drive torque of fan blade
$n$	rotational speed of fan blade	$\tau_c$	resistance torque of fan blade
$p$	pressure	$\Phi$	axial flow coefficient in fan, annulus averaged
$R$	mean fan blade radius	$\Phi_T$	flow coefficient of throttle
$R_{tip}$	fan blade tip radius	$\Psi$	total-to-static pressure rise coefficient
$s$	normalized static entropy	$\Psi_{c0}$	shut-off value of axisymmetric characteristic
$t$	time		
$U$	blade speed at mean radius		

## 1. INTRODUCTION

Ducted fans are widely used in unmanned aerial vehicles(UAV) and other vertical take-off and landing aircraft(VTOL) due to their high propulsive efficiency, low noise level and safety. Ducts can provide additional lift, with the inlet lip for ducted fans providing the lift, see [McCormick \(1999\)](#) and [Graf \(2005\)](#). During the take-off, landing and near-ground hovering of UAVs, the vicinity of the ground makes the aerodynamics of the vehicle and the fan more complex because of the influence that the ground exerts on both the UAV and the ducted fan. Extensive studies have been conducted to improve the control method and stability of the vehicle in ground effect. However, the blockage brought by the ground changes the operating conditions of the ducted fan towards the direction of a smaller mass flowrate and a higher outlet pressure, which might cause aerodynamic stability issues in the ducted fan. In this paper, the aerodynamic stability of the ducted fan, rather than the vehicle, has been investigated and discussed.

The ground effect on open propellers, such as helicopters and quadcopters, has been investigated extensively and thoroughly for many years, e.g., [Cheeseman \(1955\)](#), [Cheeseman and Bennet \(1957\)](#). This effect was shown to have a significant influence on the take-off, landing and low-altitude hovering of helicopters and quadcopters because it can increase the lift force at the same power level. Researchers have investigated the ground effect using different methods, such as theoretical aerodynamic modelling ([Xin \*et al.\*, 1999](#), [Griffiths, 2002](#), [Nathan and Green, 2012](#)), control strategies ([Nobahari and Sharifi, 2014](#), [Bernard \*et al.\*, 2017](#), [Shi \*et al.\*, 2018](#)) and experiments ([Nathan and Green, 2008](#)).

[Hosseini \*et al.\* \(2011\)](#) employed numerical calculations and a novel dipole model to investigate the ground effect on a ducted fan aircraft. The model is practical for characterizing the ground effect for online flight control. [Divitiis \(2006\)](#) proposed two aerodynamic models to study the performance of a ducted fan UAV both with and without the ground effect. Both models take into account the interaction between the air flow and the ground effect.

The aforementioned studies focused on the impact of the ground effect on the performance and stability of the helicopters and UAVs. The influence on the fan blade, especially on the aerodynamic instability, needs more attention.

Two types of instability occur in axial compressors/fans: rotating stall and surge, which are key topics in the field of aero-engines and compressors. See [Tan \*et al.\* \(2010\)](#) for a review. Numerous researchers have investigated the mechanism, modelling and control methods for the instability, e.g., [Moore and Greitzer \(1985\)](#), [Greitzer and Moore \(1986\)](#), [Moore and Greitzer \(1986\)](#), [Kuang \*et al.\* \(2017\)](#), [Mirzabozorg \*et al.\* \(2017\)](#).

The Moore-Greitzer (MG) Model was originally proposed by Moore and Greitzer to describe the dynamic response of an axial compression system during instability. The model describes and

calculates the pressure rise of the compression system, the average value and the disturbance value of the flow coefficient as a function of time by three nonlinear third-order differential equations. The MG model has been widely used in research on the instability of the compression system, e.g., axial compressors/fans and centrifugal compressors. Furthermore, the MG model has also been modified by many researchers to include different variables, e.g., [Gravdahl and Egeland \(1997\)](#).

The authors proposed a modified MG model, which could calculate and analyse the aerodynamic stability of the ducted fan in ground effect. The model calculation results were compared with three-dimensional unsteady simulations to validate and analyse the detailed flow field of the ducted fan when the instability occurred.

## 2. THE MODIFIED MOORE-GREITZER MODEL

### 2.1 The Modified MG Model

In the original MG model, the speed of the compressor is assumed to be constant. When the equivalent operating point of the compressor moves to the left of the stability line in the characteristic curves, the flow is considered to be unstable. According to the  $B$  parameter of the compression system, the instability of the compressor can assume two specific forms: the rotating stall and surge. Although the original MG model is able to describe the compressor during the post-stall transients, in order to include the transients of the speed of the compressor into the MG model, [Gravdahl and Egeland \(1997\)](#) proposed a modified MG model considering the spool dynamics.

Since  $U$  is no longer a constant in the modified MG model, the  $B$  parameter becomes a variable. The schematic diagram of the compression system is shown in Fig. 1.  $P_T$  and  $C_x$  denote the total pressure of the environment and the axial velocity of the air flow, respectively. The Inlet Pipe and the Outlet Pipe in Fig. 1 denote the duct at the upstream and the downstream of the fan, respectively. The pressure in the plenum, referred as  $p_s$ , is considered to be uniform spatially. The valve denotes the blockage effect brought by the ground.  $L_I$ ,  $L_E$  and  $L_c$  denote the lengths of different components. Other details and the derivation of the specific formulas can be found in [Moore and Greitzer \(1986\)](#), [Gravdahl and Egeland \(1997\)](#).

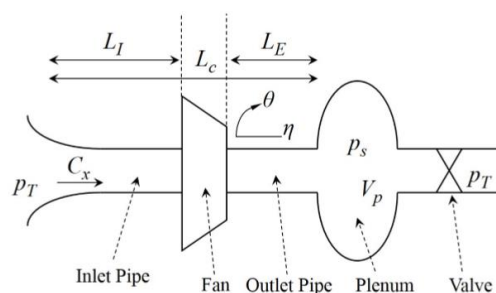


**Fig. 1. Schematic diagram of the Moore-Greitzer Model.**

After the differential equations are processed by the Galerkin method, the final expressions of the modified MG model are as follows:

$$\frac{d\Phi}{d\xi} = \frac{H}{l_c(B)} \left( -\frac{\Psi - \Psi_{c0}}{H} + 1 + \frac{3}{2} \left( \frac{\phi}{W} - 1 \right) \left( 1 - \frac{J}{2} \right) - \frac{1}{2} \left( \frac{\phi}{W} - 1 \right)^3 - \frac{l_E U_d \Gamma \Lambda_1}{bH} \Phi \right) \quad (1)$$

$$\frac{d\Psi}{d\xi} = \frac{\Lambda_2}{B} (\Phi - \Phi_T) - 2\Lambda_1 \Gamma B \Psi \quad (2)$$

$$\frac{dJ}{d\xi} = J \left( 1 - \left( \frac{\phi}{W} - 1 \right)^2 - \frac{J}{4} - \frac{2U_d \Gamma \Lambda_1 (m-1)W}{3bH} \right) \quad (3)$$

$$\frac{dB}{d\xi} = \Lambda_1 \Gamma B^2 = \Lambda_1 (u - \tau_c) B^2 \quad (4)$$

where  $\Phi$ ,  $\Psi$  and  $J$  denote the circumferentially averaged flow coefficient, the pressure rise coefficient and the squared amplitude of angular variation, respectively.  $B$  denotes the  $B$  parameter in the MG model.  $\xi$  denotes the dimensionless time, defined as  $U_d t/R$ .  $U_d$  denotes the desired velocity of the fan blade at the averaged radius.  $H$ ,  $W$  and  $\Psi_{c0}$  represent the key parameters in the performance characteristics of the compressor.  $l_c$ ,  $l_E$  and  $m$  represent the geometric characteristics of the compressor.  $J$  represents the square of the stall amplitude.  $\Lambda_1$ ,  $\Lambda_2$ ,  $a$  and  $b$  are variables defined to simplify the expressions of the differential equations.  $\Gamma$  denotes the dimensionless torque of the compressor rotor.

To properly simplify the calculation process, a P-type controller was used for the rotational speed of the compressor, the expression of which is

$$\Gamma_t = c(U_d - U) \quad (5)$$

where  $\Gamma_t$  denotes the torque output from the motor to the compressor rotor, and  $c$  denotes the control parameter of the speed controller.

After the original MG model is modified by introducing the equation of motion of the compressor rotor spool, the above model can calculate the transients of the  $B$  parameter with time and the dynamic response of the rotating stall and surge of the compression system.

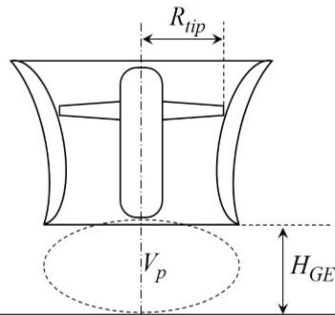


Fig. 2. Schematic diagram of the ground effect.

To further describe the ducted fan in ground effect, the parameter of height needs to be introduced in the above model. As shown in Fig. 2,  $H_{GE}$  denotes the distance between the duct outlet and the ground. To simplify the following calculation and analysis, the dimensionless height  $h$  was introduced, defined as  $H_{GE}/R_{tip}$ , where  $R_{tip}$  denotes the radius of the fan tip. Based on Hosseini *et al.* (2011), the pressure at the cylinder under the duct fan is uniformly higher than it is in the environment. Therefore, the cylinder, denoted by  $V_p$  in Fig. 2, was treated as the "plenum" in Fig. 1.

In Eq. (2),  $\Phi_T$  represents the valve flow coefficient downstream of the compressor, given by the expression

$$\Phi_T(\Psi) = \gamma_T \sqrt{\Psi} \quad (6)$$

where  $\gamma_T$  represents the throttling coefficient of the valve. In the original MG model,  $\gamma_T$  is a fixed value and is directly given by the input and  $V_p$ . In the modified MG model, both  $\gamma_T$  and  $V_p$  will be given as functions of  $h$  in the following part.

## 2.2 Identification of the Model Parameters

As described previously,  $V_p$  denotes the volume of the cylinder between the duct outlet and the ground, hence the function is written as

$$V_p = \pi \cdot R_{tip}^2 \cdot H_{GE} \quad (7)$$

After replacing  $H_{GE}$  with " $hR_{tip}$ ", Eq. (7) can be written as

$$V_p = \pi \cdot R_{tip}^3 \cdot h \quad (8)$$

To obtain the function of  $\gamma_T = f(h)$ , Eq. (6) can be written as

$$\gamma_T = f(h) = \Phi_T(\Psi) / \sqrt{\Psi} \quad (9)$$

Based on Divitiis (2006), the induced velocity of the ducted fan is the exponential of the dimensionless height. Therefore,  $f(h)$  is in the form of

$$f(h) = C_A \cdot (1 - e^{-C_B \cdot h}) \quad (10)$$

where  $C_A$  and  $C_B$  are the constants. To determine these two constants, three-dimensional simulations were conducted, which will be described in the Model Validation section. The simulation was conducted with  $h$  ranging from 0.1 to 4.0. The CFD calculation results and the fitted curve are shown in Fig. 3. The relation between  $\gamma_T$  and  $h$  can be written as

$$\gamma_T = f(h) = 1.09(1 - e^{-2h}) \quad (11)$$

The other parameters in the modified MG model are given in Table 1 based on the geometric measurements and design results of the ducted fan.

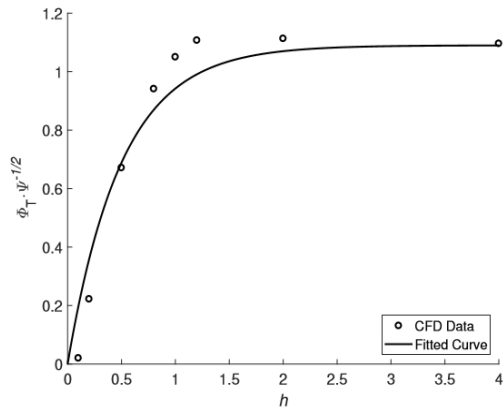


**Fig. 3. Fitted throttle coefficients with CFD results.**

**Table 1 Identification of the Parameters**

Parameter	Value
$a$	0.3
$A_c$	0.0819 m <sup>2</sup>
$a_s$	340 m/s
$H$	0.025
$I$	$1.2 \times 10^{-4}$ kg · m <sup>2</sup>
$L_c$	0.15 m
$l_E$	1.4089
$l_l$	0.1
$m$	1.25
$\Psi_{c0}$	0.021
$R$	0.09585 m
$R_{hub}$	0.0302 m
$R_{rip}$	0.1615 m
$\rho$	1.15 kg/m <sup>3</sup>
$\sigma$	0.9
$W$	0.09

Based on Table 1, the ground effect MG model could calculate the transients of the ducted fan with two more input parameters: the dimensionless height  $h$  and the desired velocity at the averaged blade radius  $U_d$ . In the present study, the two parameters determine the operating conditions of the ducted fan in ground effect. The initial value of several variables in the MG model were given as  $\Phi_0 = 0.2$ ,  $\Psi_0 = 0.06$ ,  $J_0 = 0.05$ , and  $B_0 = 0.1$ . There was a total of 3000 time steps, corresponding to 477.5 revolutions.

### 3. MODEL CALCULATION RESULTS

The aerodynamic stability of the ducted fan was first calculated during hovering with constant fan speeds and various heights by the ground effect MG model. The dimensionless height varied from  $h = 4$  to  $h = 0.2$ . The rotational speed  $n$  varies from 2000 rpm to 8000 rpm, covering the entire speed range of the ducted fan.

Two operating conditions were selected and calculated first: both cases had a rotational speed of 6000 rpm, and the heights were 0.2 and 1.2, respectively. Figure 4 and Fig. 5 are transient

signals of the mass flowrate, outlet pressure and  $J$  of the ducted fan with two heights. The horizontal axis represents the time with fan blade revolutions.

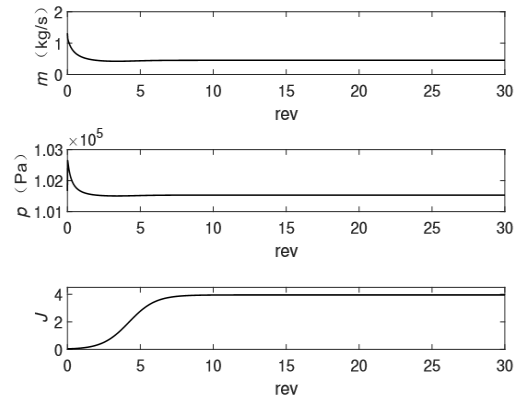


**Fig. 4. Calculated results of the ducted fan hovering with  $n = 6000$  rpm at  $h = 0.2$ .**

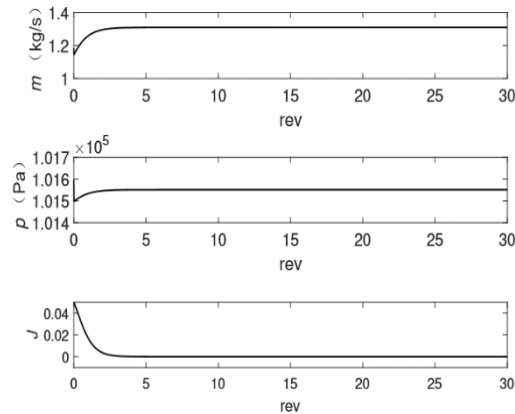


**Fig. 5. Calculated results of the ducted fan hovering with  $n = 6000$  rpm at  $h = 1.2$ .**

The stability of the compression systems could be indicated by the development of  $J$  and the mass flowrate. When  $J$  increases and remains stable at a certain value, e.g., the development in Fig. 4, a rotating stall occurs for the compressor. When  $J$  remains stable at zero, there are two possibilities. If the mass flowrate is stable, the compressor is stable as well, as shown in Fig. 5. If the mass flowrate has a periodic oscillation, a surge occurs for the compressor.

Similar calculations have been conducted with different heights and rotational speeds. The results are shown in Fig. 6. The horizontal and vertical axes represent the rotational speed and the height, respectively. The circles indicate that the ducted fan could operate stably at the corresponding points. The crossings indicate that a rotating stall occurs at the point. Figure 6 shows that the stability of the ducted fan in ground effect mainly depends on the dimensionless height rather than the rotational speed. To further demonstrate the influence of the rotational speed, the transition part near  $h = 0.49$  has been calculated in detail, as shown in Fig. 7.

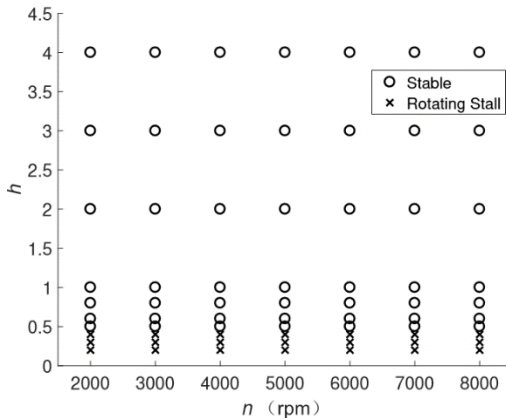


Fig. 6. Influence of different heights on the calculated stability of the ducted fan.

The crossings indicate that a rotating stall occurs at the point, while the size of the crossing denotes the speed of the rotating stall development.

Based on the calculation results of the modified MG model, several conclusions can be drawn. Comparing the mass flowrates in Fig. 4 and Fig. 5, the ground effect significantly reduces the mass flowrate of the ducted fan during the rotating stall. The angular variation  $J$  in these two cases reaches at the stable value, either in stable or rotating stall conditions, within 10 revolutions. However, based on Fig. 7, the rotating stall in the transition area might take much longer to fully develop.

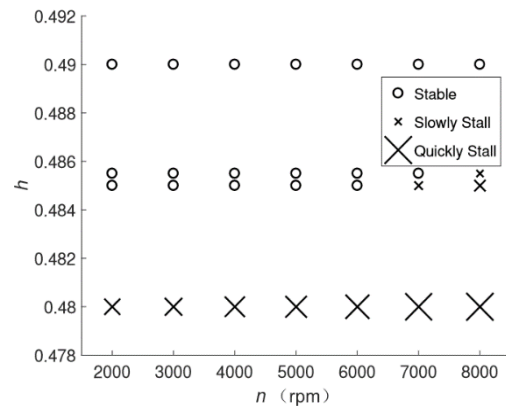


Fig. 7. Influence of different rotational speeds on the calculated stability of the ducted fan.

Between the two parameters in the modified model,  $h$  and not  $n$  dominates the stability of the ducted fan in ground effect. Although  $n$  could influence the time consumption of the rotating stall development, the effect could be neglected.

#### 4. MODEL VALIDATION BY THREE-DIMENSIONAL SIMULATION

Three-dimensional unsteady simulations were employed to investigate the detailed flow and the instability of the ducted fan in ground effect and to validate the modified MG model.

#### 4.1 Numerical Methodology

The simulation was performed using ANSYS-CFX, which is based on a three-dimensional, compressible finite volume scheme. Structural, hexahedral meshes were carefully constructed to resolve all important areas of the flow: the surface boundary area, the blade tip gap and the ground. The entire numerical domain had approximately 14 million nodes, with a  $y^+$  of smaller than 2 on the blade surfaces and the ground. Figure 8 shows the simulation domain, with the ducted fan located at the bottom of the cylinder. The bottom surface of the cylinder was set as the ground wall, and the other surfaces were the open environment. The axial location of the ground varies to create different numerical cases with different heights.

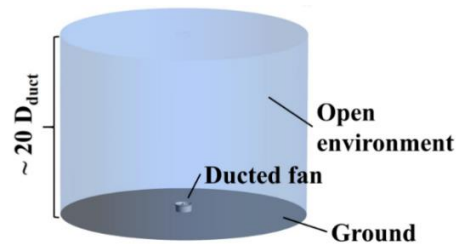


Fig. 8. Simulation domain for the ducted fan operating in ground effect.

The simulations were performed with the standard SST turbulence model provided inside the software. The convergence target was  $1 \times 10^{-6}$ . The fan was solved in the rotating frame of reference while the other parts were in a stationary frame of reference. The connection planes between the rotational domain and the stationary domain were set as "transient rotor stator" inside the software. The physical time step was  $1/20$  of each blade rotating to the position of the next one. Each physical time step consisted of 5 iterations. Transient simulations took their initial conditions from steady predictions with the same other parameters. Standard ideal air properties were used in the simulation. The ground wall, the duct surface and the hub were treated as a no-slip wall, and the open environment was given a total pressure of 101,325 Pa and a total temperature of 293 K.

#### 4.2 Simulation Case Selection and Pre-Setup

Due to the computational resource restriction, three cases were selected to conduct the unsteady simulations,  $h = 0.2$ ,  $h = 0.5$  and  $h = 1.2$ . According to the model calculation, the rotating stall occurred when  $h$  was 0.2, and the ducted fan was stable when  $h$  was 1.2. The selection of  $h = 0.5$  was due to the case located in the stability-instability transition area. The basic unsteady simulations for all three cases lasted more than 10 revolutions. However, the simulation of the unstable cases was extended by 15 more revolutions to capture the post-stall process.

The steady simulations were employed first to provide the initial state for the unsteady simulations. To capture the detailed rotating stall development process, several pressure monitor points were

located in the flow passages. As shown in Fig. 9, two blade heights, the 10% and 90% blade heights, were selected to monitor the transient pressure. The monitor points were located downstream of the blades and at the middle of the flow passages. The monitor points were fixed in the rotating frame of reference, rotating at the same speed with the fan blades.

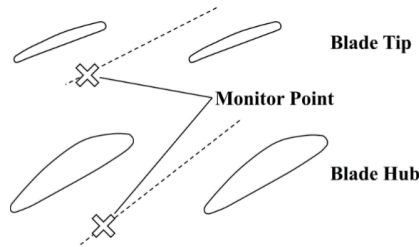


Fig. 9. Locations of the pressure monitor points.

## 5. SIMULATION RESULTS AND DISCUSSION

### 5.1 Transient Pressure Signals

Because the averaged static pressures at the duct outlet for the three cases were quite different, the relative pressure was chosen to analyse the transient pressure. The relative pressure was defined as

$$\Delta p = p - \bar{p} \quad (12)$$

where  $p$  and  $\bar{p}$  denote the transient pressure and time-averaged pressure at the monitor point, respectively.

The relative pressures at the blade tip region for the three cases are shown in Fig. 10, with different colours referring to different heights. The horizontal and vertical axes denote the time in revolutions and the relative pressures, respectively. The disturbances of the relative pressure of the three cases are quite different. The pressure of the  $h = 0.2$  case changes severely from the beginning, while the disturbance of pressure in the  $h = 0.5$  case develops gradually into periodic disturbance, and the pressure in the  $h = 1.2$  case remains nearly stable. The preliminary conclusion can be drawn that the instability occurred in the cases of  $h = 0.2$  and  $h = 0.5$ , while the  $h = 1.2$  case was stable. Based on the modified MG model result, the ducted fan is stable with  $h = 0.5$ , which is different from the simulation result.

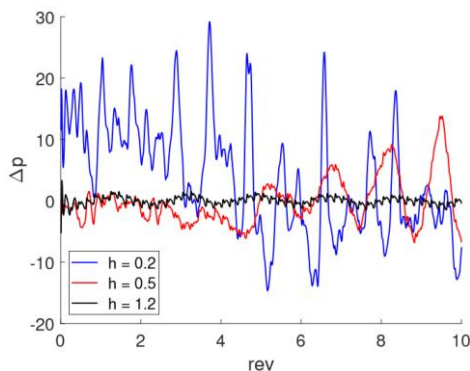


Fig. 10. Transient pressure signals at the blade tip region of three different heights.

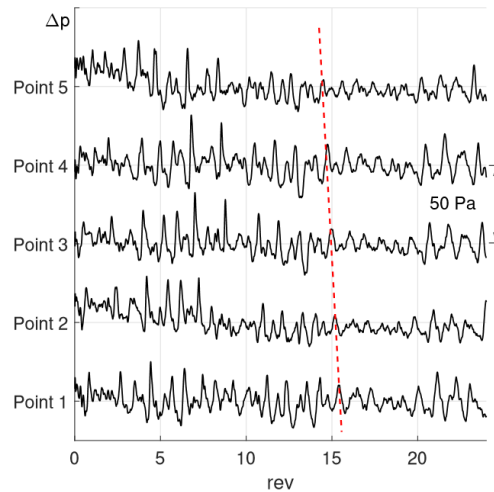


Fig. 11. Transient relative pressures of different monitor points at the blade tip region with  $h = 0.2$ .

Figures 11-14 show the relative pressure signals at the blade tip region and the hub region of the two unstable cases, respectively. Comparing the pressure signals between the tip region and the hub region, it can be shown that the disturbance amplitude at the hub region is larger than that at the tip region. However, the circumferential rotations of the pressure at the tip region are much clearer than that at the hub region, as shown by the red dashed lines in Fig. 11 and Fig. 13. Comparing Fig. 11 and Fig. 13, it can be shown that the pressure signals in the  $h = 0.2$  case are much more complicated. It is speculated that more than one stall cells appeared in the  $h = 0.2$  case, which can be proved by a detailed flow field analysis. Comparing Fig. 12 and Fig. 14, it can be found that the disturbance amplitude in the  $h = 0.2$  case is much larger than that in the  $h = 0.5$  case because the blockage caused by the ground mainly influenced the blade hub region, resulting in the circumferentially distorted pressure distribution at the duct outlet plane.

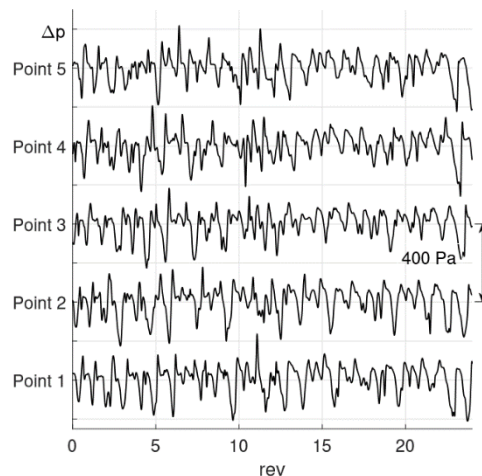
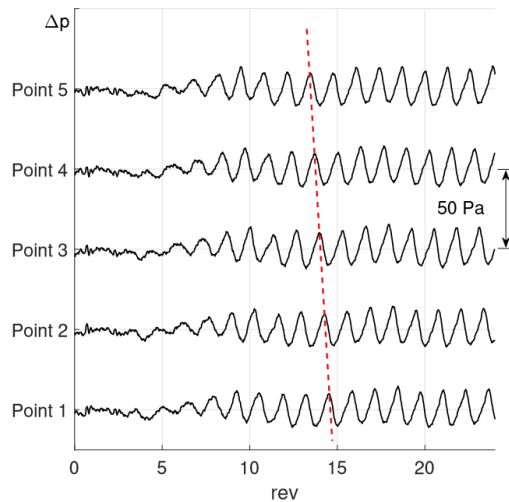
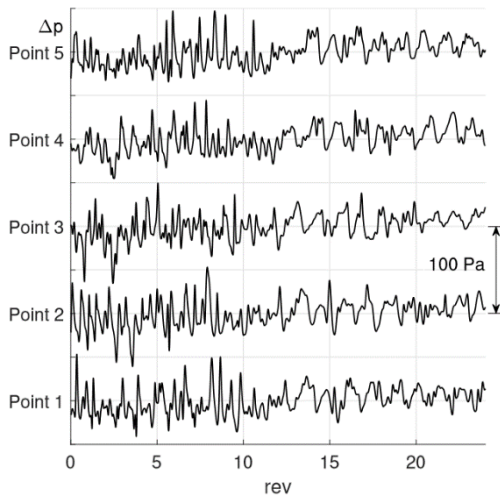


Fig. 12. Transient relative pressures of different monitor points at the blade hub region with  $h = 0.2$ .



**Fig. 13. Transient relative pressures of different monitor points at the blade tip region with  $h = 0.5$ .**



**Fig. 14. Transient relative pressures of different monitor points at the blade hub region with  $h = 0.5$ .**

The further analysis of the pressure signals was based on the Fast Fourier Transformation (FFT). The FFT result of the pressure signals at the blade tip region is shown in Fig. 15. The rotational speed of the fan blade is 6000 rpm, i.e. 100 Hz. The first blue peak appears at 78.6 Hz, which is the stall cell frequency in the rotating frame of reference corresponding to 21.4% of the blade rotational speed in the stationary frame of reference. The second blue peak appears at 157.1 Hz which is two times of the base frequency. The first red peak appears at exactly 100 Hz, the same frequency as the fan blade. Therefore, this pressure disturbance is stationary in the stationary frame of reference, which is the circumferentially distorted pressure distribution caused by the ground. The second red peak appears at 171.4 Hz, which is higher than 100 Hz, indicating that more than one stall cells exist. In summary, the typical rotating stall occurred in the  $h = 0.5$  case with a rotational speed of 21% of the blade speed. However, the  $h = 0.2$  case had two types of stall at the same time: the rotating stall with multiple stall cells and the "ground effect" stall. The latter had one stall cell,

which caused the transient pressure to act like a rotating stall, while the stall cell was stationary in the ground reference frame, i.e., the ground effect stall cell was not rotating spontaneously towards the circumferential direction.

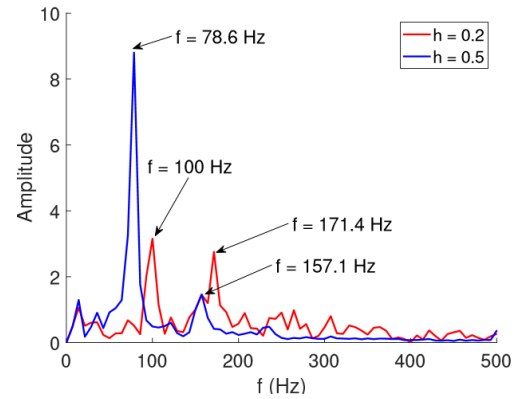


**Fig. 15. Fourier Transform results of transient relative pressure at the blade tip region.**

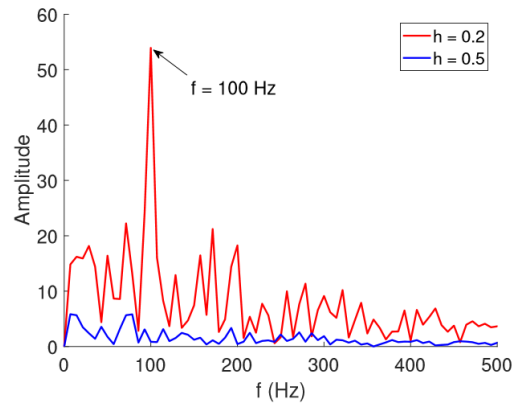


**Fig. 16. Fourier Transform results of transient relative pressure at the blade hub region.**

The FFT result of the pressure signals at the blade hub region is shown in Fig. 16. The only distinct peak appears at 100 Hz in the  $h = 0.2$  case, of which the amplitude is much larger than that in Fig. 15. Furthermore, Fig. 16 implies that (1) only a "ground effect" stall, rather than a rotating stall, occurred at the blade hub region and (2) a "ground effect" stall only occurred when  $h$  was smaller than a certain value.

## 5.2 Detailed flow field

To analyse the stall process in details, the normalised static entropy distributions downstream of the fan blades are shown in Fig. 17 and Fig. 18.

Different parts of the figure correspond to different time steps in revolutions. The normalised static entropy was defined as the local static entropy divided by the mass-averaged static entropy downstream of the fan blades. The fan blades rotate in the clock-wise direction in Fig. 17 and Fig. 18.

As shown in Fig. 13, the ducted fan was stable during the first eight revolutions. Since then, the circumferential distortion gradually developed at the

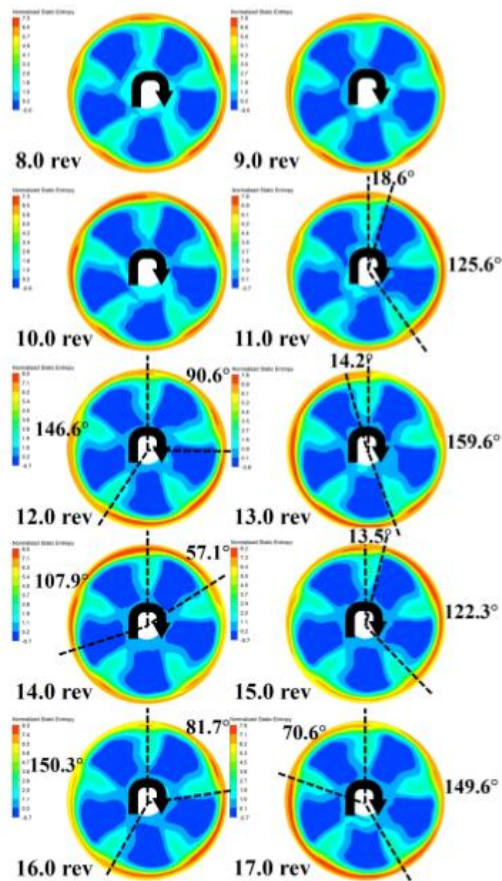


Fig. 17. Normalised entropy contours at different time steps for  $h = 0.5$ .

blade tip region. Therefore, the normalised static entropy distributions of the  $h = 0.5$  case start from 8.0 rev in Fig. 17. For 8.0 rev, 9.0 rev and 10.0 rev in Fig. 17, the static entropy is basically uniform among the different blade passages. For 11.0 rev, the distortion appears clearly in the right part. The circumferential width and the position of the rotating stall cell is labeled by the dashed lines in Fig. 17. As the fan blades rotate, the stall cell rotates in the same direction, with an approximate speed of 20%-25% of the fan, which is consistent with the FFT analysis result of 21.4%.

Similar to the  $h = 0.5$  case, the normalised static entropy distributions of the  $h = 0.2$  case are shown in Fig. 18. Since multiple stall cells appeared in the  $h = 0.2$  case, the unsteady results are shown with smaller time steps to enable a detailed analysis. Therefore, Fig. 18 starts from 10.0 rev, with a time step of 0.2 rev, rather than 1.0 rev as shown in Fig. 17.

The stall cells are much more unstable than the cells in the  $h = 0.5$  case. The circumferential locations are changing, and the amplitudes of the stall cells vary significantly. Several easily found stall cells are labelled by black dashed lines in Fig. 18. Based on the location of the bottom stall cell for 10.8 rev and its location for 11.8 rev, the rotational speed of the stall cell is also approximately 20%-25% of the fan.

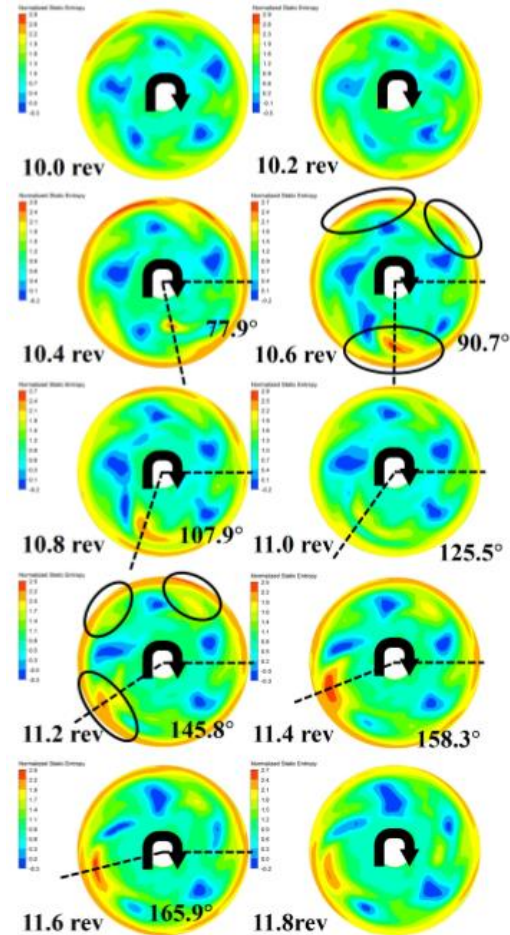


Fig. 18. Normalised entropy contours at different time steps for  $h = 0.2$ .

However, the conclusion cannot be drawn based on the FFT result in Fig. 15 due to the number of stall cells that are not clear. The stall cells merge and separate at different time steps, hence the difficulty of counting them.

## 6. CONCLUSIONS

In the present study, a modified Moore-Greitzer model considering the rotational speed and height of the ducted fan has been proposed to estimate the aerodynamic stability of the ducted fan in ground effect. To validate the model and further analyse the instability development process, three-dimensional unsteady simulations were conducted for three typical cases:  $h = 1.2$ ,  $h = 0.5$  and  $h = 0.2$ . Based on the calculation results and discussion, several conclusions can be drawn as follows:

1. The modified model is capable of estimating the aerodynamic stability of the ducted fan in ground effect. Compared with the three-dimensional numerical results, the stability critical height estimated by the model is slightly lower. Furthermore, both the model results and the simulation results need to be validated by experiments.

2. For the ducted fan in ground effect, the aerodynamic instability occurs as a rotating stall, rather than a surge. The development process of the rotating stall depends on the height and the rotational speed of the ducted fan. A smaller height and a larger rotational speed reduced the time consumption of the rotating stall development, with the height dominating the effect.
3. Based on the three-dimensional unsteady simulations, a rotating stall occurs in the ducted fan in the  $h = 0.5$  case, with only one stall cell. In the  $h = 0.2$  case, there is the combination of two stall types: a rotating stall and a ground effect stall. At the blade tip region, both types of stalls exist at the same time, while the ground effect stall dominates at the blade hub region. The transient pressure signals indicate that the ground effect stall has the same pattern with the rotating stall but remains stationary in the ground reference frame.

#### ACKNOWLEDGMENTS

The authors sincerely thank the Tsinghua-RWTH Aachen Collaborative Innovation Project. The authors are also grateful to Jinke Chen from the State Key Laboratory of Automotive Safety and Energy, who provided several critical and constructive inputs.

#### REFERENCES

- Bernard, D. D. C., F. Riccardi, M. Giurato and M. Lovera (2017). A dynamic analysis of ground effect for a quadrotor platform. *IFAC-PapersOnLine* 50(1), 10311-10316.
- Cheeseman, I. and W. Bennet (1957). *The effect of the ground on a helicopter rotor*. R & M 3021.
- Cheeseman, I. C. (1955). *The effect of the ground on a helicopter rotor in forward flight*. Technical report, Aeronautical Research Council Reports and Memoranda.
- Divitiis, N. D. (2006). Performance and stability analysis of a shrouded-fan unmanned aerial vehicle. *Journal of aircraft* 43(3), 681-691.
- Graf, W. E. (2005). *Effects of duct lip shaping and various control devices on the hover and forward flight performance of ducted fan UAVs*. Ph. D. thesis, Virginia Tech, Virginia, USA.
- Gravdahl, J. T. and O. Egeland (1997). A Moore-Greitzer axial compressor model with spool dynamics. In *Proceedings of the 36th IEEE Conference on Decision and Control, Volume 5, San Diego, California, USA*, pp. 4714-4719. IEEE: IEEE.
- Greitzer, E. and F. Moore (1986). A theory of post-stall transients in axial compression systems: part ii—application. *Journal of Engineering for Gas Turbines and Power* 108(2), 231-239.
- Griffiths, D. A. (2002). A study of dual-rotor interference and ground effect using a free-vortex wake model. In *American Helicopter Society 58th Annual Forum*, Montreal, Canada, June 11-13, 2002.
- Hosseini, Z., A. Ramirez-Serrano and R. J. Martinuzzi (2011). Ground/wall effects on a tilting ducted fan. *International Journal of Micro Air Vehicles* 3(3), 119-141.
- Kuang, H., S. W. Chu, H. Zhang and S. Ma (2017). Flow mechanism for stall margin improvement via axial slot casing treatment on a transonic axial compressor. *Journal of Applied Fluid Mechanics* 10(2), 703-712.
- McCormick, B. W. (1999). *Aerodynamics of V/STOL flight*. Massachusetts, USA: Courier Corporation.
- Mirzabozorg, M. A. S., M. Bazazzadeh and M. Hamzade (2017, JAN). Numerical study on the effect of single shallow circumferential groove casing treatment on the flow field and the stability of a transonic compressor. *Journal of Applied Fluid Mechanics* 10(1, 2), 257-265.
- Moore, F. and E. Greitzer (1985). *A theory of post stall transients in multistage axial compression systems*. US. NASA contractor rep..
- Moore, F. K. and E. M. Greitzer (1986). A theory of post-stall transients in axial compression systems: Part i—development of equations. *Journal of engineering for gas turbines and power* 108(1), 68-76.
- Nathan, N. and R. Green (2008). Measurements of a rotor flow in ground effect and visualization of the brown-out phenomenon. In *64th American Helicopter Society Annual Forum*.
- Nathan, N. D. and R. B. Green (2012). The flow around a model helicopter main rotor in ground effect. *Experiments in Fluids* 52(1), 151-166.
- Nobahari, H. and A. Sharifi (2014). Continuous ant colony filter applied to online estimation and compensation of ground effect in automatic landing of quadrotor. *Engineering Applications of Artificial Intelligence* 32, 100-111.
- Shi, G., X. Shi, M. O'Connell, R. Yu, K. Azizzadenesheli, A. Anandkumar, Y. Yue and S. J. Chung (2018). *Neural lander: Stable drone landing control using learned dynamics*. arXiv preprint arXiv:1811.08027.
- Tan, C., I. Day, S. Morris and A. Wadia (2010). Spike-type compressor stall inception, detection, and control. *Annual review of fluid mechanics* 42, 275-300.
- Xin, H., J. Prasad and D. Peters (1999). Dynamic inflow modeling for simulation of a helicopter operating in ground effect. In *Modeling and Simulation Technologies Conference and Exhibit*, pp. 4114.